Numerical investigation of an in-situ observed flow regimes during solidification of an NH_4Cl – 70 wt%H_2O solution

IOP Conf. Series: Materials Science and Engineering **861** (2020) 012041 doi:10.1088/1757-899X/861/1/012041

Numerical investigation of an in-situ observed flow regimes during solidification of an NH_4Cl – 70 wt%H_2O solution

M Wu, M Stefan-Kharicha, A Kharicha and A Ludwig

Chair for Simulation and Modelling of Metallurgical Processes, Dept. of Metallurgy, University of Leoben, A-8700 Leoben, Austria

E-mail: menghuai.wu@unileoben.ac.at

Abstract. A volume-average mixed columnar-equiaxed solidification model, where the dendritic morphology of crystals is described with the dendrite envelope, was developed by the current authors. As an evaluation effort, this model is used to simulate a solidification experiment of ammonium chloride water (NH_4Cl – 70 wt%H_2O) solution. The solution was cooled in a water cooled copper mould (10×8×1 cm^3), and the solidification process and the flow dynamics during solidification were in-situ observed/recorded with a Particle Imagine Velocimetry technique. The striking features of solidification in this experiment are that the crystal morphology is dominant in columnar structure, and typical 4 flow regimes in the bulk solution during solidification appear: pure thermal convection (TH), unstable (turbulent) flow caused by double diffusive convection (TU), turbulent-stratified flow (TU-ST), meandering flow (MF). These flow regimes correspond to different cooling/solidification stages, and reflect their interactions with the developing mushy zone. The calculated solidification sequence and the flow dynamics (4 flow regimes) agree with the experimental ones. The experimentally observed phenomena were successfully explained by the simulation.

1. Introduction

Volume-average based multiphase approach was introduced by Beckermann and co-workers to model the solidification problem by bridging the transport phenomena at different length scales [1-2]. A concept of "dendrite envelope", as introduced by Rappaz and Thevoz [3-4], was also incorporated into the volume-average approach by Wang and Beckermann to consider the dendritic crystal morphology during solidification [5]. Recently, this work was extended by Wu and Ludwig to consider the mixed columnar-equiaxed solidification in a five-phase solidification model [6-7]. This model was evaluated by comparison with in-situ solidification experiments on organic materials [8] and also on metal castings [9-10]. A primary goal of this conference paper is to further evaluate the model by comparison with solidification experiment of ammonium chloride water (NH4Cl – 70 wt%H2O) solution. A more ambitious goal is to explain the experimentally observed flow phenomena, by correlating each of them with the solidification structure in the advancing mushy zone, hence to achieve deeper understanding of the flow-solidification interaction.

2. Experimental setup and numerical model

2.1. Experimental setup and material data

An in-situ experiment on solidification of the NH_4Cl – 70 wt%H_2O solution was made [11]. The solution was cooled in a mould (10×8×1 cm^3) from an initial temperature 314.15 K. The mould top is open to the air (heat transfer coefficient 12 W/m2/K); the side/bottom walls are water-cooled with imposed temperature ($T_{\text{Wall}} = 2.69\times10^{-6}t^2 - 2.488\times10^{-2}t + 314.15$) until reaching the lowest limit of 276.6 K;

the front/back walls are glass (adiabatic). One key solidification feature with this experiment setting is the columnar crystal morphology. A Particle Imagine Velocimetry (PIV) technique was used to record the flow dynamics. The columnar tip front was recorded by a light camera, whose image (darkness) indicated the solid volume fraction in the mushy zone. Material properties are listed in table 1.

Table 1. Material properties and other parameters

	Symbol	**Units**	**Value**	**Sources**
Thermodynamic parameter (local linearized phase diagram)				
Nominal concentration	c_0	wt% H_2O	70.43	[12]
Liquidus temperature	T_{liq}	K	304.15	[12]
Melting point of solvent	T_f	K	638.7	extrapolation
Eutectic composition	c_{eu}	wt%	0.803	[12]
Eutectic temperature	T_{eu}	K	257.267	[12]
Liquidus slope	m	K (wt%)$^{-1}$	-4.75	[12]
Equilibrium partition coefficient	k	-	0.0	[12]
Gibbs Thomson coefficient	Γ	K.m	4.0×10^{-8}	[13]
Thermo-physical properties				
Reference density	ρ_ℓ , ρ_s	kg·m^{-3}	1073	[14]
Specific heat	c_p^ℓ , c_p^s	J kg^{-1} K^{-1}	3249	[15]
Thermal conductivity of liquid	k_ℓ	W m^{-1} K^{-1}	0.468	[15]
Thermal conductivity of solid	k_s	W m^{-1} K^{-1}	2.7	[15]
Latent heat	Δh_f	J kg^{-1}	3.18×10^5	[15]
Viscosity	μ_ℓ	Kg m^{-1} s^{-1}	1.3×10^{-3}	[15]
Diffusion coefficient (solid)	D_s	m^2 s^{-1}	8.0×10^{-13}	estimation
Diffusion coefficient (liquid)	D_ℓ	m^2 s^{-1}	4.8×10^{-9}	[15]
Boussinesq parameters				
Liquid thermal expansion coefficient	β_T	K^{-1}	3.9×10^{-4}	[14]
Liquid solutal expansion coefficient	β_C	wt%$^{-1}$	2.87×10^{-3}	[14]
Dendrite morphology				
Primary dendritic arm spacing	λ_1	m	6.0×10^{-4}	[11]
Secondary dendritic arm spacing	λ_2	m	1.0×10^{-4}	[11]

2.2. Brief model description

The mixed columnar-equiaxed solidification model as developed by the current author has considered five phases [6-7]. As dominant columnar dendritic structure is observed in this experiment, a simplified version with pure columnar growth structure is applied. Two hydrodynamic phases are considered: the primary liquid melt (ℓ) and columnar phase (c), and their volume fractions sum up to unit ($f_\ell + f_c = 1.0$). Only one set of Navier-Stokes equations are solved for the velocity of the primary liquid melt ($\bar{u}_\ell$); the velocity of the columnar phase ($\bar{u}_c$) is set as zero (stationary). The flow permeability (K) of the mushy zone, derived from the Carman-Kozeny law, refers to Ramirez *et al.* [16]; and it is a function of f_ℓ and λ_1.

As shown in figure 1, a smooth hypothetical contour connecting primary (or primary, secondary and tertiary) dendrite tips, called dendrite envelope, is constructed to separate the inter-dendritic melt and primary (extra-dendritic) melt. With this concept, the system includes three thermodynamic phases: the solid dendrites (f_s^c), the inter-dendritic melt inside the envelope (f_d^c), and the extra-dendritic

melt (identical to the primary melt f_ℓ), where $f_s^c + f_d^c = f_c$. The shape of the columnar dendrite envelope is further simplified as a cylinder with cross-section-area equivalent to the columnar tree trunk envelope (figure 1). Two morphological parameters are necessarily defined to describe the geometry of the dendrite envelope: the shape factor Φ_{env}^c and circularity factor Φ_{circ}^c. Assuming that the growth kinetics of the dendrite tips follows the LGK model [17], where the stability constant is $\sigma^* = 1/(4\pi^2)$, from the tip growth velocities ($v_{tip''}^c$) one can calculate the lateral growth velocity of the cross-section-area equivalent cylinder ($v_{env}^c = \Phi_{env}^c \cdot v_{tip''}^c$). Φ_{circ}^c is defined to relate the true diffusion area of the dendrite envelope with the area of the equivalent cylinder, $S_{env,D}^c = S_{env,M}^c / \Phi_{circ}^c$. Both shape factors are here assumed and further verified for this experiment per numerical parameter studies: Φ_{env}^c=0.7979, Φ_{circ}^c=0.33. The columnar primary dendrite tip front is tracked according to the growth kinetics of LGK model [6-7, 17].

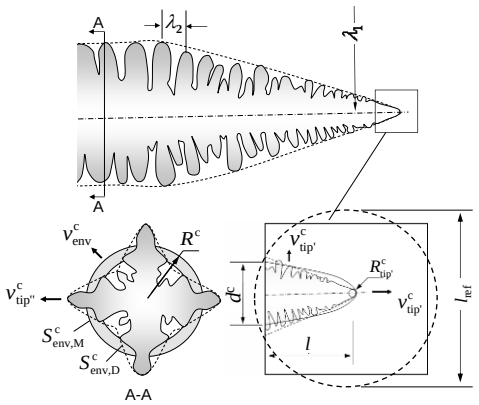

Figure 1. The shape of the columnar tree trunk envelope is simplified as a cylinder with cross-section-area equivalent to the columnar tree trunk envelope (dashed line), which connects the secondary and tertiary dendrite tips. The contour of the columnar envelope near the primary dendrite tip (dashed line connecting the primary and secondary dendrite tips) is simplified as a paraboloid.

3. Simulation – experiment comparison

The simulation was made in full 3D with average mesh size of 0.7 mm. The calculated solidification sequence and flow patterns, in comparison with the experimental results, are shown in figure 2. According to the experimental report [11], 4 typical flow patterns corresponding different cooling/solidification stages are observed. They are successfully reproduced by the numerical simulation, despite of the slight difference in the timing of the starting point for each pattern/stage. The applied thermal boundary conditions for the simulation are not perfectly in light with the experiment. In order to explain the mechanism of each flow pattern, some key solidification quantities, which mostly influence the flow, are shown in figure 3. They are the temperature (T_ℓ), solute (H_2O) concentration in the melt (c_ℓ in mass fraction), density of the melt (ρ_ℓ), volume fraction of the solid dendrite (f_s^c). The density of the melt is calculated as $\rho_\ell = \rho_{ref}\left(1-\beta_T\left(T_\ell - T_{ref}\right) - \beta_c\left(c_\ell - c_{ref}\right)\right)$.

During the early cooling stage before the start of solidification, figure 2(a), it is the thermal convection regime (TH). The flow is laminar and symmetrical: downward along the side wall and upward in the mould centre. Note that the PIV technique is not able to detect the velocity near the wall, hence the largest velocity along the side walls as predicted by the simulation was missing in the experiment.

As solidification starts, NH_4Cl crystals grow from the side/bottom walls. The mushy zone is very porous, and the maximum f_s^c in the mush is about 0.12. The rejection of solute (H_2O) in the mushy region leads to the "density reversion" [18], i.e. the melt density along the side wall becomes lighter than that in the bulk region. To the moment of 900 seconds, as shown in figure 2(b), the flow direction along the side wall is reversed, namely upwards. As shown in figure 3(a1)-(a4), temperature along the side wall is lower, while the solute concentration is higher. Balancing the thermal and solutal effect, the melt density there is smaller than the bulk region, leading to the upward melt flow, which brings

less-denser melt from lower region along the wall (through porous mushy region) to the top region. The solute rejection from the mushy zone along the bottom wall tends to rise as well, driving many plumes (or freckle trails [18]). A typical double diffusive convection pattern occurs. To this moment the flow pattern becomes chaotic. This flow regime is called turbulent regime (TU). The previous study demonstrated that the Rayleigh number due to solute-buoyancy could reach the order of magnitude of 10^{10}, larger than the turbulence criterion 10^9, but most regions were observed as laminar with very large and coherent structures.

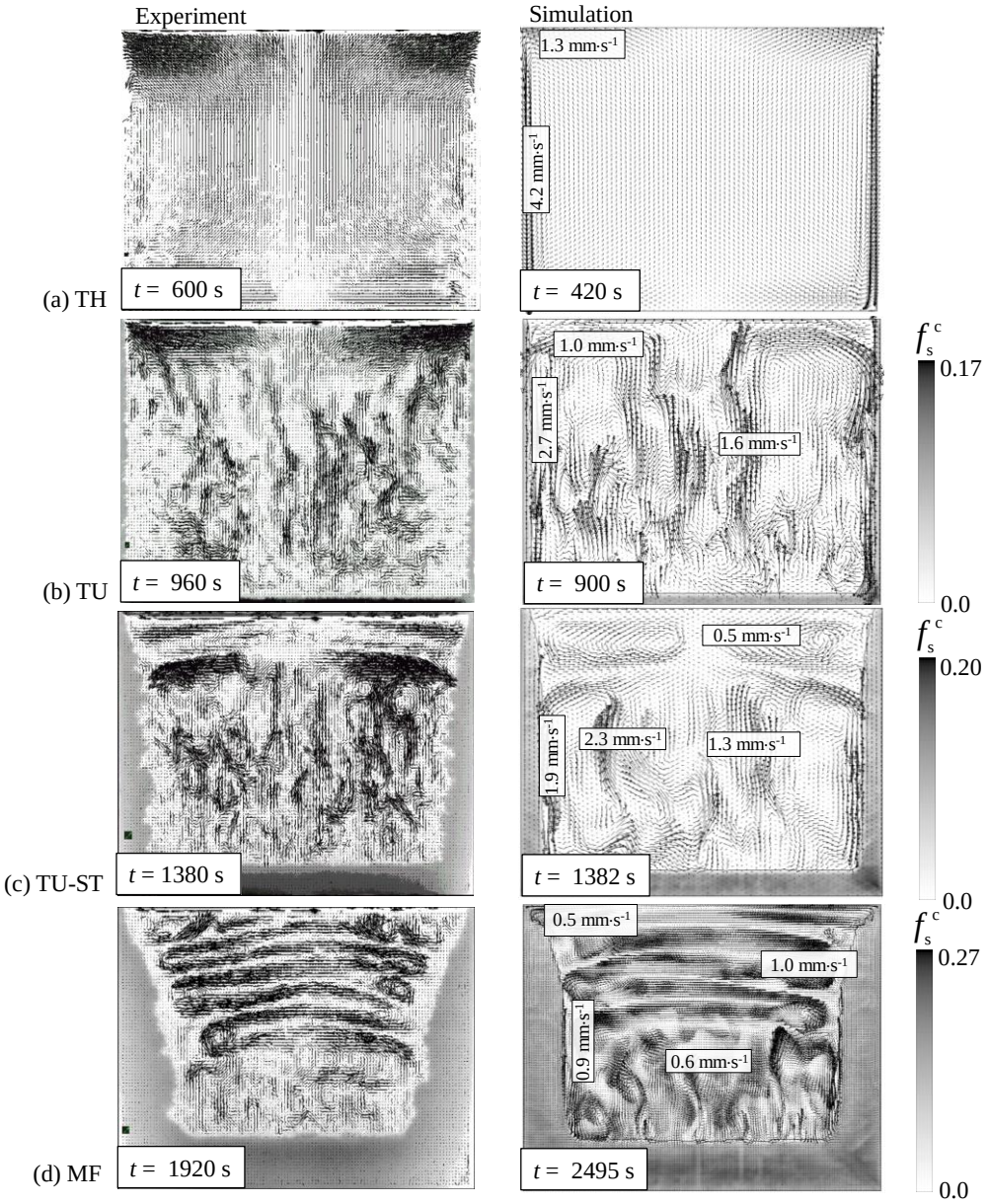

Figure 2. Solidification sequence and flow patterns in different stages: simulation-experiment comparison. Experiment (left): with grey area for the mushy zone and vectors for the measured velocity field with PIV technique. Simulation (right): with grey scale for f_s^c (volume fraction of solid dendrites) and vectors for the liquid velocity $\bar{u}_\ell$. 4 different flow patterns, which correspond to 4 different cooling/solidification stages, are: (a) TH (thermal convection)

(b) TU (turbulence) (c) TU-ST (turbulence – stratified flow) and (d) MF (meandering flow). All simulation results and the flow measurement were taken from the symmetry section.

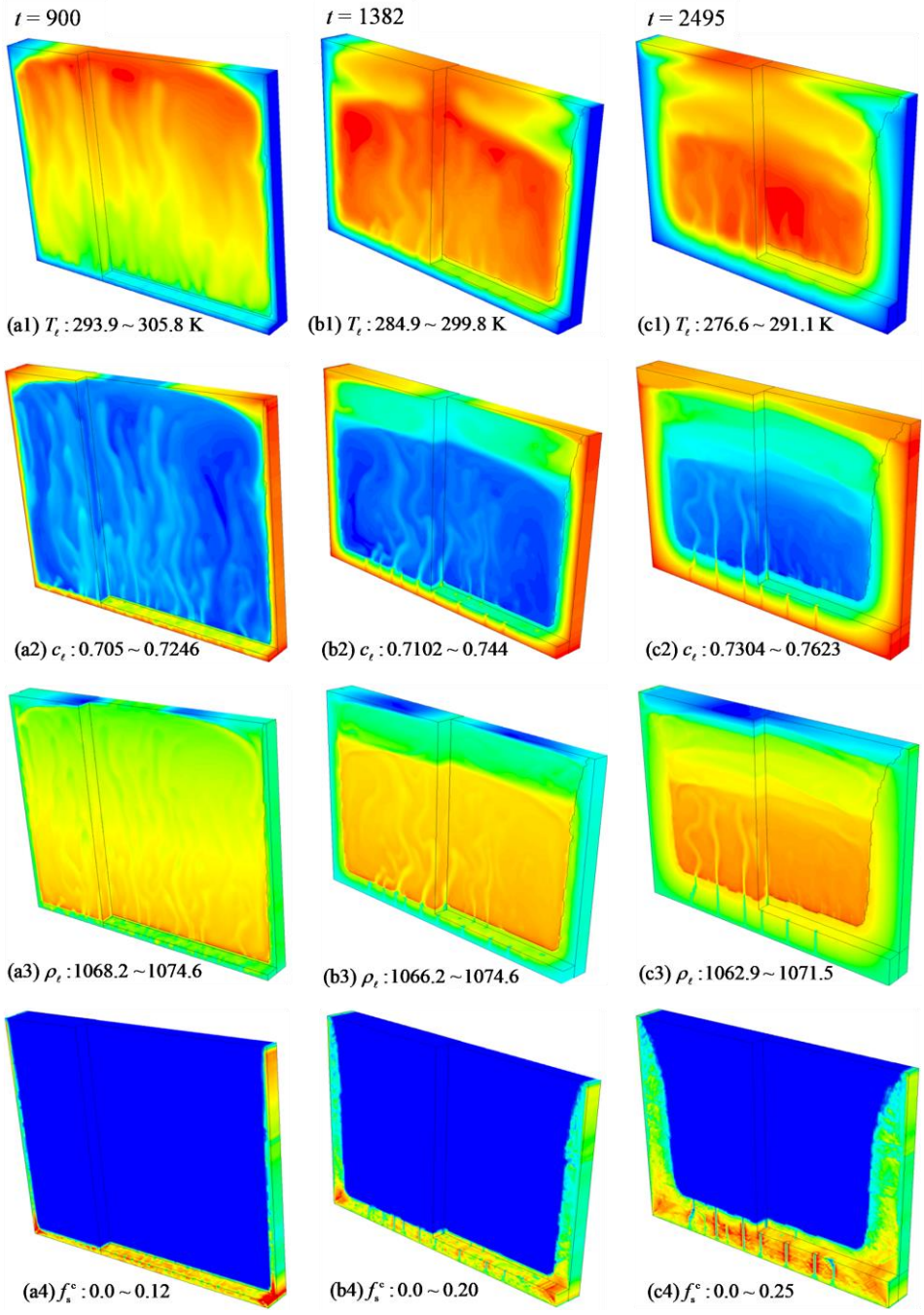

Figure 3. Some key solidification quantities (T_ℓ , c_ℓ , ρ_ℓ , f_s^c), which mostly influence the flow, are shown in a sequence at the time 900, 1382 and 2495 s. The results are shown in 3D, therefore, one can only see the distribution of each quantity in selected sections. All quantities are shown in colour scale with blue for the minimum value and red for the highest value, which are given below each figure.

To the moment ca. 1380 s, figure 2(c), the flow pattern in the mould seems divided into two parts: the lower part is similar to the previous TU region, i.e. chaotic with coherent structures, while the upper part starts a flow stratification with two symmetrical circulation loops. This flow regime is called

turbulent – stratified flow region (TU-ST). As shown in figure 3(b1)-(b4), the upward melt flow in the mushy zone along the side wall brings continuously the lighter melt (lower temperature and higher concentration of H_2O) from lower part to the upper part, leading to a separation of the bulk melt region into two parts, namely the upper part with lighter melt and the lower part of denser melt. Along the bottom wall, plumes continue to develop. The distribution of f_s^c is non-uniform, which hints the onset of freckle trails [18]: lower solid fraction inside the channel and high solid fraction in the rim regions. From the experiment, however, no stable channel was observed. This is probably due to the narrow range of f_s^c distribution, which is not detectable by the light camera.

During the late stage of solidification, figure 2(d) and figure 3(c1)-(c4), a so-called meandering flow regime (MF) is developed. The stratification flow pattern in the upper part of the mould is gradually organized horizontally in several layers in a structure of snake. Figure 4 shows more details of the flow structure for the moment of 2495 s. Generally, both simulation and experiment agree with each other very well. The reason for the snake-like MF is as follows. With the continuing of the TU-ST regime, the upper part of lower-density region becomes broader, more circulation loops are built from both sides of the mould. Gradually, the circulation loops from two sides join together, and re-arrange the flow from both sides, leading to the snake-like MF. The experiment seems to show more flow layers than those of the simulation, which is probably due to that the numerical grid resolution is not high enough. Most freckle trails develop vertically upwards; some of them become inclined and later on merged with the neighbouring ones; and some of them disappear.

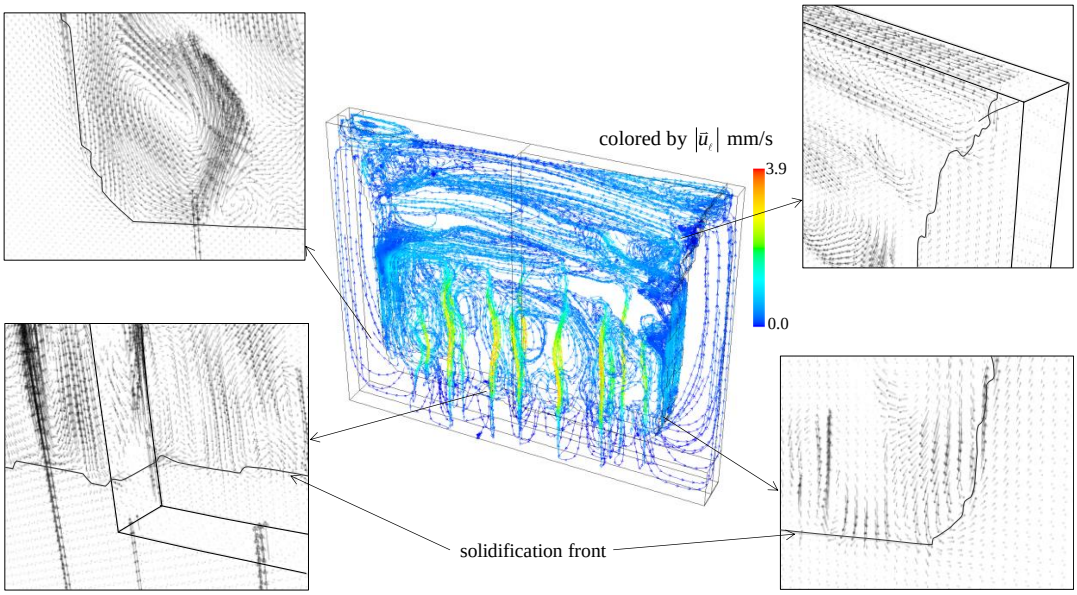

Figure 4. Flow pattern at the moment 2495 s is shown in streamlines ($|\vec{u}_\ell|$ in mm/s) and vectors as zoomed in some regions. The solidification front (position of columnar tips) is also marked with thin line. Flow in the mush is active, but with less intensity. In the bottom part of the mushy zone, the flow in some locations is still relatively strong, where plume develops.

4. Discussions and outlook

Volume-average approach was developed to model the solidification process at the macroscopic scale when the formation of as-cast structure (columnar, equiaxed zones) and macrosegregation is of primary interest [1-2, 19]. The global multiphase flow/transport phenomena are key important at the process scale. To find an experiment, which is able to record the flow at the process scale and in the meantime to record the dendrite grow at the microscopic scale, as a purpose to evaluate above volume-average model is extremely difficult. The in-situ solidification experiment based on X-ray radioscopy, which

has been used to detect both flow and crystal growth during solidification [20], is not suitable for evaluate the volume-average model as the experiment is limited to a sample thickness of ca. 100 μm (Hele-Shaw cell). Checking the as-cast structure and final macrosegregation profile with the post-mortem analysis of engineering/laboratory castings [9-10] is the most frequently used method to evaluate the volume-average model, but the global multiphase flow/transport phenomena, the key information for the formation of as-cast structure and macrosegregation, cannot be verified. Therefore, the experiment with in-situ observation of solidification of the NH_4Cl – 70 wt%H_2O solution provides the most efficient way to evaluate volume average model with following merits: (1) it can record of the flow quantitatively; (2) the sample (mould) size of the experiment is at the similar scale of engineering castings; (3) the solidification front (partial mushy zone) can be tracked.

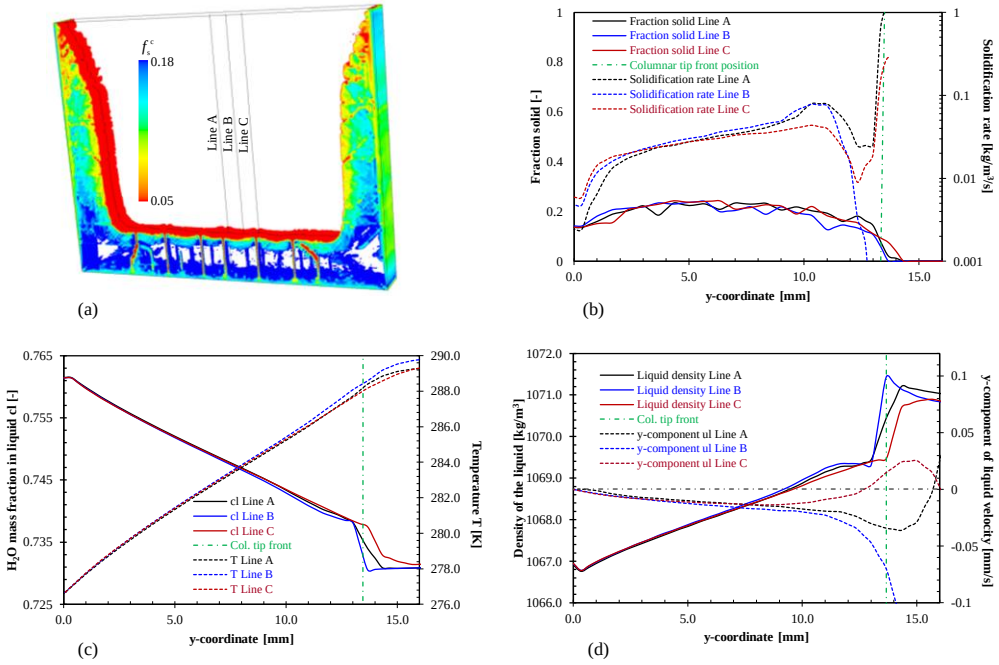

Figure 5. Formation of freckle trails at the moment 2495 s. (a) Iso-surface of f_s^c (= 0.18) indicating the position of solidification front and the formation of freckle trails; (b)-(d) distributions of 6 different quantities along 3 vertical lines (Lines A, B, C, as marked in figure (a)) in y-coordinate direction are shown: fraction solid f_s^c [-], solidification rate M_{ds}^c (kg/m^3/s), H_2O mass fraction in liquid [-], temperature [K], density of the liquid ρ_ℓ [kg/m^3], velocity component in y-coordinate direction $u_{\ell,y}$ [m/s].

All experimental data as provided in [11] were proven to be reproducible by the current volume average model, e.g. figure 2; and the embedded solidification mechanisms can be explained by analysing the modelling results in detail, figures 3-4. Furthermore, the modelling results can also be used to explain some interdendritic flow phenomena during the formation of freckle trail, as experimentally measured by Chen [21] based on a similar experiment with NH_4Cl – 74 wt%H_2O and NH_4Cl – 70 wt%H_2O solutions. Chen used dye ($KMnO_4$) injection and X-ray tomography methods to observe the flow pattern and fraction solid distribution in the mushy zone during solidification. Following findings/statements were made by Chen [21]: the upward plume in the chimneys (channels) induced a downward flow into the mush; with the development of the chimney, solid fraction around the rim of the chimney increased; however, the solid fraction at the bottom of the mushy layer remained low *through an unknown mechanism*; as a consequence, the flow in the chimney was maintained by drawing liquid downward through the mush, then in the horizontal streams along the bottom. Freckle trails

in the current experimental setting are simulated and shown in figure 4 and figure 5(a). In order to explain the experiment of Chen's with the current model, further solidification quantities/parameters along 3 vertical lines (A, B and C, in figure 5(a)) are shown in figure 5(b)-(d). The simulation confirms the experimental phenomena that (1) the liquid velocity component in the bottom mushy zone is downward (negative value), except for those which is exactly located in the freckle trails; (2) the solid fraction increases from the solidification front into the middle of the mush, then it decreases towards the bottom wall. The downward flow in the bottom mushy zone can reduce the solidification driven force (constitutional undercooling), leading a reduction of the solidification rate and allowing the flow more easy in the horizontal streams along the bottom mushy zone to feed the upward flow in the freckle trails. "Density reversion" as reported by [18] was also verified near the solidification front.

Further numerical analyses and parameter studies were carried out, e.g. the competing growth between neighboring freckle trails (seen in figure 5(a)); the influence of the crystal morphological parameters (the shape factor Φ^{c}_{env} and circularity factor Φ^{c}_{circ}) on the flow dynamics in the interdendritic region and in the bulk; the effect of the mushy permeability, or the description of permeability by different laws; the formation of crystal fragments (source of equiaxed) as favoured by the flow (plumes/chimneys). These studies would lead to a deeper understanding of the embedded mechanisms of the formation of as-solidified structure and freckle trails. However, they cannot be included in this proceeding article due to the page limit.

Acknowledgement

This work was financially supported by the Austrian Science Fund (FWF, I 4278-N36), FFG Austrian Space Application Program (ASAP, 859777), FFG Bridge I (868070).

References

[1] Beckermann C and Viscanta R 1993 *Appl. Mech. Rev*. **46** 1-27
[2] Beckermann C and Wang C 1995 *Annu. Rev. Heat Trans.* **6** 115-98
[3] Rappaz M and Thévoz P 1987 *Acta Metall*. **35** 1478-97
[4] Rappaz M and Thévoz P 1987 *Acta Metall*. **35** 2929-33
[5] Wang C and Beckermann C 1996 *Metall. Trans. A* **27** 2754-64
[6] Wu M, Fjeld A and Ludwig A 2010 *Comp. Mater. Sci*. **50** 32-42
[7] Wu M, Ludwig A and Fjeld A 2010 *Comp. Mater. Sci*. **50** 43-58
[8] Sturz L, Wu M, Zimmermann G, Ludwig A and Ahmadein M 2015 *IOP Conf. Series: Mater. Sci. Eng.* **84** 012086
[9] Ahmadein M, Wu M, Li J, Schumacher P, Ludwig A 2013 *Metall. Mater. Trans. A* **44** 2895-903
[10] Ahmadein M, Wu M and Ludwig A 2015 *J. Crystal Growth* **417** 65-74
[11] Stefan-Kharicha M, Kharicha A, Wu M and Ludwig A 2014 *Fluid Dyn. Res*. **46** 041424
[12] Stefan-Kharicha M, Kharicha A, Mogeritsch, Wu M and Ludwig A 2018 *J. Chem. Eng. Data* **63** 3170-83
[13] Ramani A and Beckermann C 1997 *Scripta Materialia* **36** 633-8
[14] Perry R, Green D and Maloney J 1999 *Perry's Chem. Engineers' Handbook*, 7th ed. The McGraw-Hill Companies: New York
[15] Beckermann C and Wang C 1996 *Metall. Mater. Trans. A* **27** 2784-95
[16] Ramirez J and Beckermann C 2003 *Metall. Mater. Trans. A* **34** 1525-36
[17] Lipton J, Glicksman M and Kurz W 1984 *Mater. Sci. Eng*. **65** 57-63
[18] Copley S, Giamei A, Johnson S, Hornbecker M 1970 *Metall. Trans.* **1** 2193-203
[19] Wu M, Ludwig A and Kharicha A 2019 *Metals* **9** 229
[20] Shevchenko N, Boden S, Gerbeth G and Eckert S 2013 *Metall. Mater. Trans. A* **44** 3797-808
[21] Chen CF 1995 *J. Fluid Mech*. **293** 81-98